

Tensile or compressive plastic deformation of cylinders assisted by cyclic torsion

Z. MRÓZ¹⁾, K. KOWALCZYK-GAJEWSKA¹⁾, J. MACIEJEWSKI¹⁾,
R. B. PECHERSKI^{1,2)}

¹⁾*Institute of Fundamental Technological Research PAS
Świętokrzyska 21, 00-049 Warsaw, Poland*

²⁾*Institute of Structural Mechanics, Faculty of Civil Engineering
Cracow University of Technology
Warszawska 24, 31-155 Cracow, Poland*

TECHNOLOGICAL METAL FORMING processes of extrusion, forging and rolling with imposed cyclic torsion or shear deformation have been recently studied in view of their advantages with respect to monotonic loading processes, cf. BOCHNIAK and KORBEL [2–4]. The present work is aimed to analyze such process in the case of simple tension or compression of a cylindrical tube with imposed cyclic torsional deformation. The material element response is assumed to be rigid-perfectly plastic or elastic-perfectly plastic. For these models, the analytical solutions can be provided for the steady cyclic responses and the effect of two process parameters, namely the ratio of shear and axial strain rates η and the amplitude of shear strain γ_m , can be clearly demonstrated. Three different regimes of cyclic response can be visualized in the plane η, γ_m . The cyclic response of a cylinder under combined axial compression and cyclic torsion is predicted by considering a simplified model of a set of concentric tubes and neglecting their radial stress interaction. The axial force and torsional moment are then specified by averaging the responses of consecutive tubes. The cyclic response diagrams for the cylinder are then generated in terms of axial force and torsional moment related to axial deformation and angle of twist.

1. Introduction

IN RECENT YEARS there has been a growing interest in the metal forming processes assisted by cyclic loading. The so-called KOBO-type forming proposed by KORBEL and BOCHNIAK [2–4, 13] and applied to extrusion of tubes and wires has demonstrated essential advantages with respect to classical forming processes. The significant reduction of required load for forming, growth of ductility, possible reduction of the dissipated energy of forming and finer grain structure are the main beneficial factors, cf. also KONG *et al.* [11, 12].

At the micro-mechanical scale, it is observed that destabilization of the developed dislocation substructure occurs with subsequent generation of coarse slip

bands propagating in a transgranular mode, thus reducing the stress level required for progressive deformation. Such effects of instabilities of hardened states at large plastic deformation were discussed already by BASIŃSKI and JACKSON [1, 7]. Also COFFIN [8] noted in his work that imposed cyclic deformation could be applied to facilitate the progressive metal forming process.

The present work is aimed at studying such cyclic deformation-assisted process by applying simple constitutive models of plastic response of metals. Our objective is to provide an analytical solution of the steady cyclic deformation process and discuss the effect of two basic parameters η and γ_m , representing, the ratio of shear and axial strain rates and the shear strain amplitude. The analysis will be carried out for a perfectly plastic material model satisfying the Huber–Mises yield condition. The types of steady cyclic responses are presented by the interaction diagrams in the plane γ_m, η . Both the piecewise linear and harmonic shear strain controls are considered. The plastic dissipation in axial and torsional straining is presented and referred to the dissipation in the monotonic tension or compression process.

The study will be pertained to a circular cylinder or tube axially deforming with a specified rate and subjected to alternating twist with specified rate and amplitude. Most cyclic loading experiments available in literature have been performed at the specified axial stress values in order to study the ratchetting strain induced by cyclic torsion. The numerous formulations of constitutive models assumed combined isotropic and kinematic hardening rules with account for recovery effects. Here we mention some papers by MRÓZ [14], MRÓZ and RODZIK [15], TRĄMPCZYŃSKI and MRÓZ [18], CHABOCHE [5], OHNO and WANG [16], KANG *et al.* [9], KHOEI and JAMALI [10], PORTIER *et al.* [17] where further references can be found. In this paper we shall refer to the tests performed by BOCHNIAK and KORBEL [2] and GROSSMAN [6] for the case of tension or compression of cylindrical specimens with imposed cyclic torsion. The analysis will be presented first for a case of cylindrical tube and next the response of a cylinder will be predicted by superposing solutions for a set of tubes of decreasing radii. The analysis with account for material hardening and recovery effects will be presented in a separate paper.

2. Problem formulation for a thin-walled tube

Consider a thin-walled tube of initial radius r_0 , length l_0 and wall thickness t_0 , subjected to axial tension or compression. Assume the axial strain rate to be specified and constant. The alternating torsion is imposed in order to reduce the axial stress and the applied axial force in order to execute the process. Denote by ε_x and γ_{xy} the axial and shear strain components and their rates by $\dot{\varepsilon}_x, \dot{\gamma}_{xy}$. The Cauchy stress components referred to the actual configuration are σ_x, τ_{xy} .

For simplicity, first the small strain formulation is considered which can next be improved by considering configuration changes for large compressive or tensile strains (see difference in Fig. 1b).

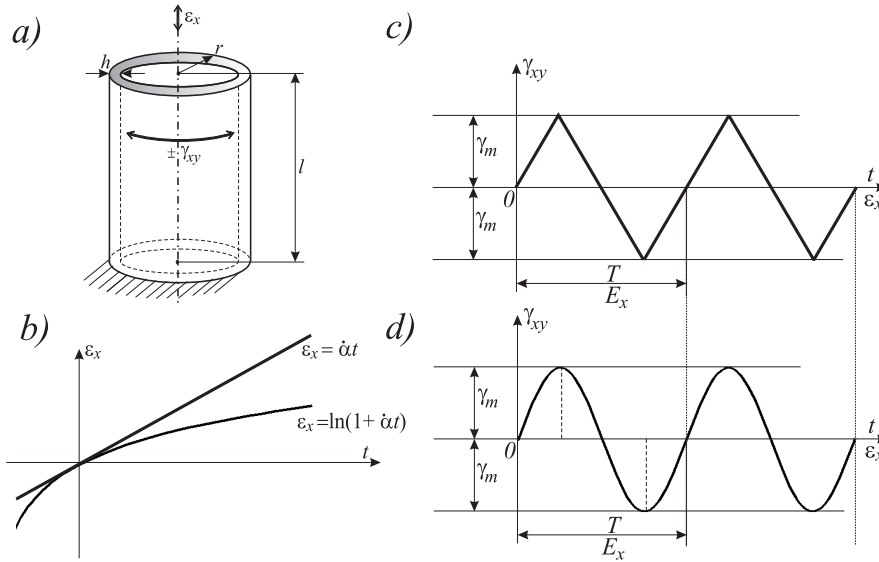


FIG. 1. Axial and torsional deformation program: a) tube dimensions, b) longitudinal strain $\varepsilon_x(t)$, c) piecewise linear variation of shear strain, d) harmonic variation of shear strain $\gamma_{xy}(t)$.

The deformation program is shown in Fig. 1. For uniform in time length variation ($l = l_0(1 \pm \dot{\alpha}t)$), the axial strain and strain rate are $|\varepsilon_x| = \dot{\alpha}t$, $|\dot{\varepsilon}_x| = \dot{\alpha}$, where $\dot{\alpha} = |\dot{l}|/l_0$. The shear strain is assumed to oscillate within the range $2\gamma_m$ and the period T . For piecewise linear oscillation, Fig. 1c, we have $\dot{\beta} = \dot{\gamma}_{xy} = 4\gamma_m/T$. Denote the ratio of rates of shear and axial strains by η , thus

$$(2.1) \quad \eta = \frac{\dot{\beta}}{\dot{\alpha}} = \text{const}, \quad \dot{\beta} = \frac{4\gamma_m}{T}, \quad \dot{\beta} > 0, \quad \dot{\alpha} > 0.$$

For the harmonic variation of γ_{xy} , Fig. 1d, we can write

$$\gamma_{xy} = \gamma_m \sin\left(\frac{2\pi}{T}t\right), \quad \dot{\gamma}_{xy} = \frac{\pi}{2}\dot{\beta} \cos\left(\frac{2\pi}{T}t\right),$$

and the ratio of strain rates is

$$(2.2) \quad \frac{\dot{\gamma}_{xy}(t)}{|\dot{\varepsilon}_x|} = \eta \frac{\pi}{2} \cos\left(\frac{2\pi}{T}t\right) = \eta \frac{\pi}{2} \cos\left(\frac{2\pi}{T} \frac{|\varepsilon_x|}{\dot{\alpha}}\right) = \eta \frac{\pi}{2} \cos\left(2\pi \frac{|\varepsilon_x|}{E_x}\right),$$

where $E_x = 4\gamma_m/\eta$ is the strain period corresponding to time period T . Let us note that the time measure can be replaced by the axial strain $|\varepsilon_x| = \dot{\alpha}t$.

In this paper we have assumed the uniform extension or compression of tube and the piecewise linear or harmonic shear strain control. Such programs were executed in experimental works [2] and [6].

3. Deformation analysis for a rigid-perfectly plastic material model

To understand the constitutive model assumptions in the analysis of cyclic response of a tube, we provide the analytical solution for the elastic-perfectly plastic material model assuming the Huber–Mises yield condition and the associated flow rule. The constitutive equations can be written in the form:

- yield condition

$$(3.1) \quad F = \sqrt{\sigma_x^2 + 3\tau_{xy}^2} - \sigma_0 = 0,$$

- rate equations

$$(3.2) \quad \begin{aligned} \dot{\varepsilon}_x &= \dot{\varepsilon}_x^e + \dot{\varepsilon}_x^p = \frac{\dot{\sigma}_x}{E} + \dot{\lambda} \frac{\sigma_x}{\sigma_0}, \\ \dot{\gamma}_{xy} &= \dot{\gamma}_{xy}^e + \dot{\gamma}_{xy}^p = \frac{\dot{\tau}_{xy}}{G} + \dot{\lambda} \frac{3\tau_{xy}}{\sigma_0}, \end{aligned}$$

where $\dot{\lambda} \geq 0$, $F \leq 0$, $\dot{\lambda}F = 0$, $\dot{F}\dot{\lambda} = 0$. Here ‘dot’ denotes the rate with respect to the process evolution parameter, such as increasing axial strain, E and G are the elastic Young and Kirchhoff moduli and σ_0 denotes the yield stress.

In this section we shall analyse the rigid-perfectly plastic material. Neglecting elastic strains, from (3.2) we have

$$(3.3) \quad \dot{\varepsilon}_x = \dot{\varepsilon}_x^p = \dot{\lambda} \frac{\sigma_x}{\sigma_0}, \quad \dot{\gamma}_{xy} = \dot{\gamma}_{xy}^p = \dot{\lambda} \frac{3\tau_{xy}}{\sigma_0}.$$

Inverting (3.3), the dissipation function can be specified, namely

$$\dot{D} = \sigma_x \dot{\varepsilon}_x^p + \tau_{xy} \dot{\gamma}_{xy}^p = \sigma_0 \dot{\lambda} = \sigma_0 \sqrt{(\dot{\varepsilon}_x^p)^2 + \frac{1}{3}(\dot{\gamma}_{xy}^p)^2}$$

and

$$(3.4) \quad \begin{aligned} \sigma_x &= \frac{\partial \dot{D}}{\partial \dot{\varepsilon}_x^p} = \sigma_0 \frac{\dot{\varepsilon}_x^p}{\sqrt{(\dot{\varepsilon}_x^p)^2 + \frac{1}{3}(\dot{\gamma}_{xy}^p)^2}}, \\ \tau_{xy} &= \frac{\partial \dot{D}}{\partial \dot{\gamma}_{xy}^p} = \sigma_0 \frac{\frac{1}{3}\dot{\gamma}_{xy}^p}{\sqrt{(\dot{\varepsilon}_x^p)^2 + \frac{1}{3}(\dot{\gamma}_{xy}^p)^2}}. \end{aligned}$$

For the piecewise-linear shear strain oscillation, Fig. 1c, we obtain from (3.4)

$$(3.5) \quad \sigma_x = \frac{\sigma_0}{\sqrt{1 + \frac{\eta^2}{3}}}, \quad \tau_{xy} = \pm \frac{\eta}{3} \frac{\sigma_0}{\sqrt{1 + \frac{\eta^2}{3}}}$$

and the specific dissipation power equals

$$(3.6) \quad \dot{D} = \sigma_0 |\dot{\varepsilon}_x| \sqrt{1 + \frac{\eta^2}{3}} = \dot{D}_0 \sqrt{1 + \frac{\eta^2}{3}}, \quad \dot{D}_0 = \sigma_0 |\dot{\varepsilon}_x|.$$

For the harmonically varying shear strain, in view of (2.2), we obtain the stress components in the plastic state

$$(3.7) \quad \begin{aligned} \sigma_x &= \frac{\sqrt{3}\sigma_0}{\sqrt{3 + \eta^2 \frac{\pi^2}{4} \cos^2 \left(2\pi \frac{|\varepsilon_x|}{E_x} \right)}}, \\ \tau_{xy} &= \frac{\eta}{3} \frac{\sqrt{3}\sigma_0 \eta^2 \frac{\pi}{2} \cos \left(2\pi \frac{|\varepsilon_x|}{E_x} \right)}{\sqrt{3 + \eta^2 \frac{\pi^2}{4} \cos^2 \left(2\pi \frac{|\varepsilon_x|}{E_x} \right)}} \end{aligned}$$

and the dissipation power is expressed as follows:

$$(3.8) \quad \dot{D} = \sigma_0 |\dot{\varepsilon}_x| \sqrt{1 + \eta^2 \frac{\pi^2}{12} \cos^2 \left(2\pi \frac{|\varepsilon_x|}{E_x} \right)} = \dot{D}_0 \sqrt{1 + \eta^2 \frac{\pi^2}{12} \cos^2 \left(2\pi \frac{|\varepsilon_x|}{E_x} \right)}.$$

Some interesting conclusions can be drawn from this simple analysis. For the case of piecewise linear shear strain control, the stress path AB at constant axial stress value corresponds to consecutive combined plastic flow periods followed

by rigid unloading to a reverse shear straining point on the yield surface, Fig. 2a. The shear hysteresis loop is shown in Fig. 2b and the axial stress variation in Fig. 2c. It follows from (3.5) and (3.6) that the axial stress value depends on η and is always reduced, whereas the dissipation power increases with increasing η . For instance, for $\eta = 3$, there is $\sigma_x = \frac{1}{2}\sigma_0$ and $\dot{D} = 2\dot{D}_0 = 2\sigma_0|\dot{\epsilon}_x|$. Thus, the axial stress reduction occurs at the expense of increasing dissipated energy in the deformation process.

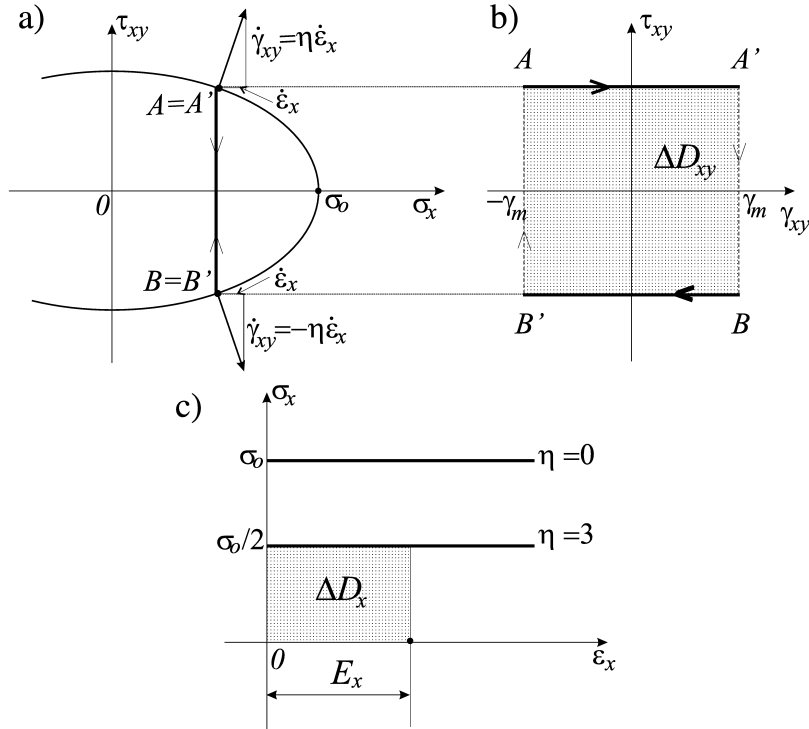


FIG. 2. Piecewise linear shear strain control: a) stress path, b) shear stress-strain hysteresis loop, c) axial stress variation.

The harmonic shear strain control provides a different stress path $ACBC'$ following the yield surface, Fig. 3a. Thus, there is no unloading stage and the deformation process proceeds in a *fully plastic regime*. The shear stress-strain hysteresis loop is shown in Fig. 3b. The axial stress varies between the values corresponding to A or B and the maximal value $\sigma = \sigma_0$ at C , Fig. 3c. The stress-strain path in Fig. 3c touches the line $\sigma = \sigma_0$ at C, C', C'', \dots . Note that this line corresponds to $\eta = 0$, that is to monotonic axial straining. The dissipation power increases with respect to its value $\dot{D}_0 = \sigma_0|\dot{\epsilon}_x|$ corresponding to pure axial deformation.

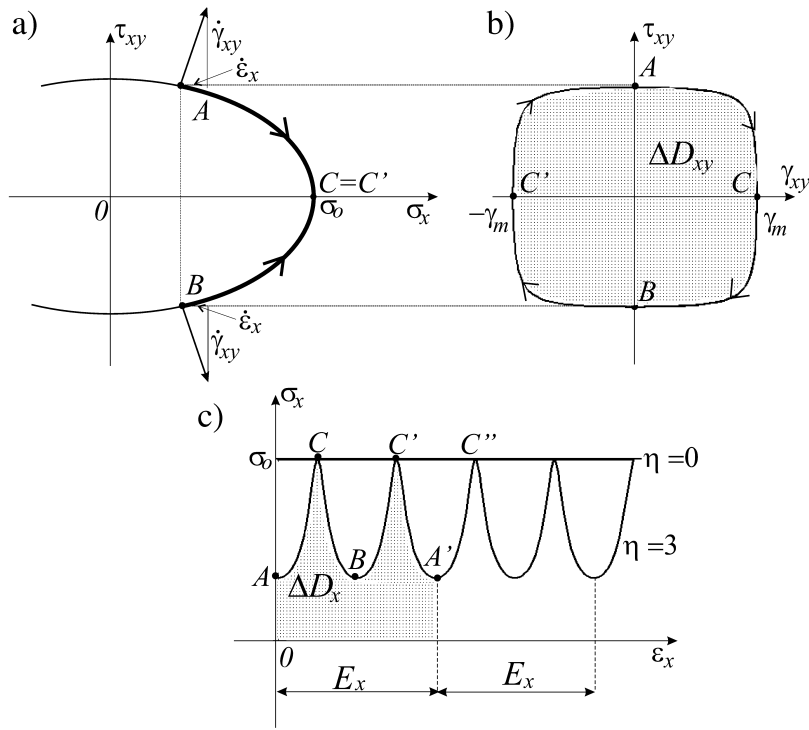


FIG. 3. Harmonic shear strain control: a) stress path, b) shear stress-strain hysteresis loop, c) axial stress variation.

To illustrate the dissipated energy variation with process parameters, let us calculate the dissipated energy in tension and torsion modes during one cycle of deformation. For the piecewise linear shear strain control, in view of (3.5) we have

$$(3.9) \quad D_c^\gamma = \int_0^{\text{cycle}} \tau_{xy} d\gamma_{xy} = \frac{3}{4} \eta \frac{\sigma_0 \gamma_m}{\sqrt{1 + \frac{1}{3} \eta^2}} = \sigma_0 E_x \frac{\frac{\eta^2}{3}}{\sqrt{1 + \frac{\eta^2}{3}}},$$

$$(3.10) \quad D_c^\varepsilon = \int_0^{\text{cycle}} \sigma_x d\varepsilon_x = \sigma_0 E_x \frac{1}{\sqrt{1 + \frac{\eta^2}{3}}},$$

where D_c^γ and D_c^ε are the dissipated energies in torsion and axial strain cycles. The total dissipated energy per cycle equals

$$(3.11) \quad D_c^t = D_c^\gamma + D_c^\varepsilon = \sigma_0 E_x \sqrt{1 + \frac{\eta^2}{3}} = D_0^t \sqrt{1 + \frac{\eta^2}{3}}.$$

Similarly, introducing $e = |\varepsilon_x|/E_x$, for the case of harmonic control of shear strain, in view of (2.2), (3.7) and (3.8), we obtain

$$D_c^\gamma = \int_0^{\text{cycle}} \tau_{xy} d\gamma_{xy} = \sigma_0 E_x \int_0^1 \frac{\eta^2}{3} \frac{\frac{\pi^2}{4} \cos^2(2\pi e)}{\sqrt{1 + \frac{\eta^2 \pi^2}{3} \frac{\pi^2}{4} \cos^2(2\pi e)}} de,$$

$$D_c^\varepsilon = \int_0^{\text{cycle}} \sigma_x d\varepsilon_x = \sigma_0 E_x \int_0^1 \frac{1}{\sqrt{1 + \frac{\eta^2 \pi^2}{3} \frac{\pi^2}{4} \cos^2(2\pi e)}} de,$$

and

$$D_c^t = \sigma_0 E_x \int_0^1 \sqrt{1 + \frac{\eta^2 \pi^2}{3} \frac{\pi^2}{4} \cos^2(2\pi e)} de.$$

Figure 4 presents the variation of dissipated energies per one cycle in axial and torsional deformation. It is seen that the dissipated energy portion D_c^ε decreases with the increasing cycle frequency, but the dissipated energy D_c^γ increases. This leads to a total dissipated energy increase during the uniaxial deformation process.

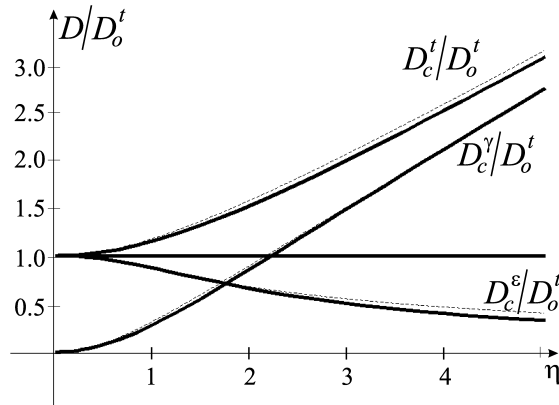


FIG. 4. Variation of the dissipated energy in one deformation cycle with the strain rate ratio η : continuous line – piecewise linear shear strain control, dashed line – harmonic shear strain control.

4. Cyclic solution for an elastic-perfectly plastic material

Consider now the elastic-plastic material model for which the constitutive equations are specified by (3.1) and (3.2). We shall analyze both the piecewise linear and harmonic shear strain controls.

4.1. Piecewise linear shear strain control: analytical solution

In view of the constraint $\dot{\gamma}_{xy}/\dot{\epsilon}_x = \eta$, from (3.2) it follows that

$$(4.1) \quad \dot{\sigma}_x = E \left(\dot{\epsilon}_x - \dot{\lambda} \frac{\sigma_x}{\sigma_0} \right), \quad \dot{\tau}_{xy} = G \left(\eta \dot{\epsilon}_x - \dot{\lambda} \frac{3\tau_{xy}}{\sigma_0} \right).$$

For the plastic state, the consistency condition requires that

$$(4.2) \quad \dot{F} = \sigma_x \dot{\sigma}_x + 3\tau_{xy} \dot{\tau}_{xy} = 0.$$

Substituting (4.1) into (4.2), we obtain

$$(4.3) \quad \dot{\lambda} = \sigma_0 \frac{E\sigma_x + 3G\eta\tau_{xy}}{E\sigma_x^2 + 9G\tau_{xy}^2} \dot{\epsilon}_x, \quad \dot{\lambda} > 0, \quad \dot{\epsilon}_x > 0.$$

Let us note that η takes positive and negative values, however, the shear stress τ_{xy} changes its sign with η , so we have $\tau_{xy} > 0$, $\eta > 0$ and $\tau_{xy} < 0$, $\eta < 0$, so that $\tau_{xy}\eta > 0$. The inverse elastic-plastic equations are

$$(4.4) \quad \begin{aligned} \dot{\sigma}_x &= E \left(1 - \frac{E\sigma_x + 3G\eta\tau_{xy}}{E\sigma_x^2 + 9G\tau_{xy}^2} \sigma_x \right) \dot{\epsilon}_x, \\ \dot{\tau}_{xy} &= G \left(\eta - \frac{E\sigma_x + 3G\eta\tau_{xy}}{E\sigma_x^2 + 9G\tau_{xy}^2} 3\tau_{xy} \right) \dot{\epsilon}_x \end{aligned}$$

and for the elastic path we have

$$\dot{\sigma}_x = E\dot{\epsilon}_x, \quad \dot{\tau}_{xy} = G\dot{\gamma}_{xy} = G\eta\dot{\epsilon}_x.$$

To integrate analytically the rate equations (4.4), let us introduce the trigonometric stress representation satisfying the yield condition (3.1), namely

$$(4.5) \quad \sigma_x = \sigma_0 \cos \theta, \quad \sqrt{3}\tau_{xy} = \sigma_0 \sin \theta$$

with the rates

$$(4.6) \quad \dot{\sigma}_x = -\sigma_0(\sin \theta)\dot{\theta}, \quad \sqrt{3}\dot{\tau}_{xy} = \sigma_0(\cos \theta)\dot{\theta}.$$

The first incremental equation (4.4) can now be presented as follows:

$$(4.7) \quad \frac{\sigma_0}{3G}\dot{\theta} = \frac{\frac{\sqrt{3}\eta}{3} \cos \theta - \sin \theta}{1 + \left(\frac{3G}{E} - 1 \right) \sin^2 \theta} \dot{\epsilon}_x.$$

Let us introduce the following notation:

$$(4.8) \quad \tan \Phi = \frac{\sqrt{3}|\eta|}{3} = \frac{\dot{\gamma}_{xy}}{\dot{\varepsilon}_x}, \quad m = \frac{3G}{E} - 1 = \frac{1 - 2\nu}{2(1 + \nu)},$$

$$\bar{\varepsilon}_x = \frac{E}{\sigma_0} \varepsilon_x = \frac{\varepsilon_x}{\varepsilon_0}, \quad \bar{\gamma}_{xy} = \frac{E}{\sigma_0} \frac{\gamma_{xy}}{\sqrt{3}}, \quad \tan \varphi = (1 + m) \tan \Phi$$

where $\varepsilon_0 = \sigma_0/E$ is the elastic strain in uniaxial tension associated with the yield stress σ_0 . Equation (4.7) can now be rewritten in the incremental form

$$(4.9) \quad d\bar{\varepsilon}_x = \frac{\cos \Phi}{1 + m} \cdot \frac{1 + m(\sin \theta)^2}{\sin(\pm \Phi - \theta)} d\theta.$$

Integrating (4.9), we obtain for $\eta = \pm|\eta|$

$$(4.10) \quad \bar{\varepsilon}_x = C + \underbrace{\frac{\cos \Phi}{1 + m} \left[m \cos(\Phi \pm \theta) - (1 + m(\sin \Phi)^2) \ln \left| \tan \frac{\Phi \pm \theta}{2} \right| \right]}_{f(\pm\theta)}$$

where C is the integration constant obtained from the initial values on the respective paths.

Using trigonometric stress representation one may also integrate ε_x^p and the rate of plastic dissipation to obtain the plastic strain and dissipation energy. The results are collected in the Appendix.

For the elastic path, we can write for $\eta = \pm|\eta|$

$$(4.11) \quad s_x = \frac{\sigma_x}{\sigma_0} = \frac{E\varepsilon_x}{\sigma_0} + s_0 = \bar{\varepsilon}_x + s_0,$$

$$s_{xy} = \frac{\sqrt{3}\tau_{xy}}{\sigma_0} = \frac{\sqrt{3}G\eta}{\sigma_0} \varepsilon_x + t_0 = \pm \tan \varphi \bar{\varepsilon}_x + t_0.$$

4.2. Analysis of process parameters

Consider now the steady-state cyclic deformation process for specified γ_m and η . Figure 5a presents one of the typical steady cyclic states in the stress plane $s_x = \sigma_x/\sigma_0$, $s_{xy} = \sqrt{3}\tau_{xy}/\sigma_0$. The yield condition is now represented by a circle of unit radius and the conjugate plastic strain rates are ε_x^p and $\dot{\gamma}_{xy}^p/\sqrt{3}$.

The cyclic stress path is formed by two semi-cycles $O^* - D - A - O^*$ and $O^* - B - C - O^*$, where the position O^* is specified by the value $s_x = s^*$ which is to be determined. The elastic stress paths AB and CD are inclined at the angle φ to the s_x -axis, where for positive η

$$\tan \varphi = \frac{\dot{s}_{xy}}{\dot{s}_x} = \frac{\sqrt{3}\dot{\tau}_{xy}}{\dot{\sigma}_x} = (1 + m) \tan \Phi = \left(\frac{3}{2} \frac{1}{1 + \nu} \right) \frac{\eta}{\sqrt{3}}$$

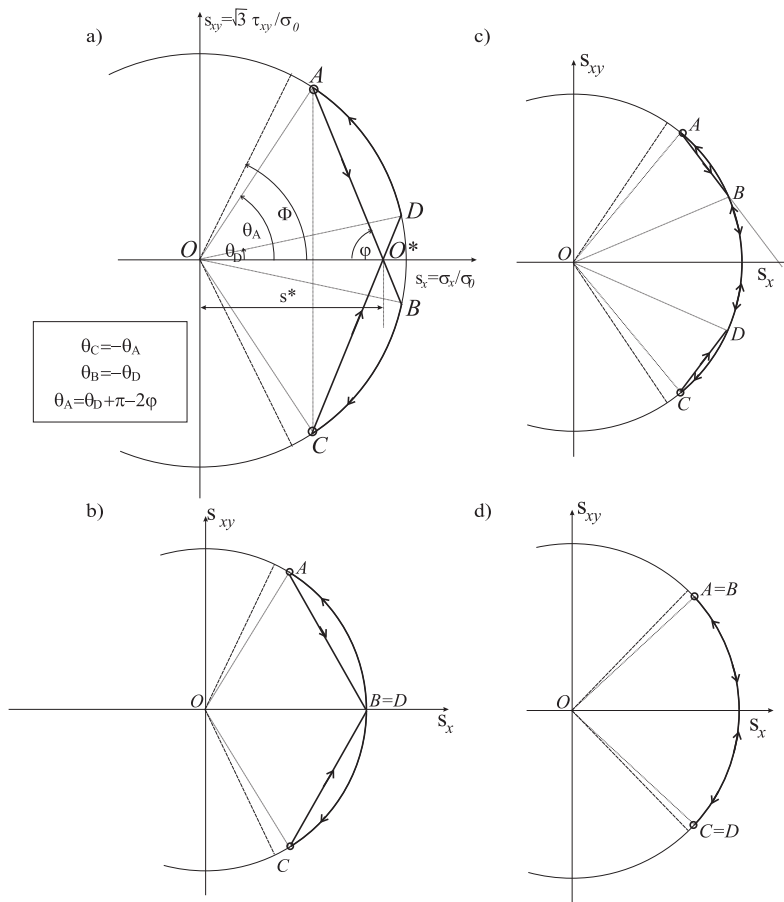


FIG. 5. Steady state cycles representation in the s_x, s_{xy} -plane a) the case $\eta > \eta_m(\gamma_m)$, b) the case $\eta = \eta_m(\gamma_m)$, c) the case $\eta_l(\gamma_m) < \eta < \eta_m(\gamma_m)$, d) the case $\eta > \eta_l(\gamma_m)$.

and the angle Φ specifies purely plastic strain path for transformed strains $\bar{\varepsilon}_x$ and $\bar{\gamma}_{xy}$. Note that $\varphi > \Phi$ for $\nu \leq 0.5$. The radial lines $O - A$ and $O - D$ are inclined at the angles θ_A and θ_D to the s_x -axis. From geometrical relations it is seen that

$$\Delta\theta = \theta_A - \theta_D = \pi - 2\varphi, \quad (4.12)$$

$$\tan \theta_A = \frac{\sin \varphi \sqrt{1 - (s^*)^2 \sin^2 \varphi} - s^* \cos \varphi}{\cos \varphi \sqrt{1 - (s^*)^2 \sin^2 \varphi} + s^* \sin^2 \varphi}.$$

Let us specify first the limit value of η for which the elastic unloading or reloading occurs along the path AB or CD . The elastic unloading is specified by $\dot{\lambda} = 0$ and

$$\dot{F} = \sigma_x \dot{\sigma}_x + 3\tau_{xy} \dot{\tau}_{xy} = \sigma_x (E \dot{\varepsilon}_x) + 3\tau_{xy} (-G |\eta| \dot{\varepsilon}_x) \leq 0,$$

where $\sigma_x = \sigma_0 \cos \theta_A$, $3\tau_{xy} = \sqrt{3}\sigma_0 \sin \theta_A$. For $\dot{F} = \dot{\lambda} = 0$ the neutral, limit process is observed. At the point of reversion of the deformation path we have

$$(4.13) \quad \dot{F} = \left(\cos \theta_A - \sqrt{3} \sin \theta_A \frac{G}{E} \eta \right) \sigma_0 E \dot{\varepsilon}_x = (1 - (2 + m)(\sin \Phi)^2) \sigma_0 E \dot{\varepsilon}_x \leq 0$$

where we have assumed the limit value of $\theta_A = \Phi$ occurring for $\gamma_m \rightarrow \infty$. For finite shear amplitude values, there should be $\theta_A < \Phi$. The inequality (4.13) provides

$$|\eta| \geq \sqrt{\frac{3}{1+m}} = \eta_{l(\infty)}$$

and for finite values of γ_m the corresponding limit value $\eta_l = \eta_l(\gamma_m)$ should be greater than $\eta_{l(\infty)}$, thus

$$\eta_l(\gamma_m) > \eta_{l(\infty)}.$$

The other steady cycle pattern can be generated when the points D and B merge on the s_x -axis, Fig. 5b. Then, the maximal axial stress reached in the cyclic process equals the static value σ_0 . Considering the elastic path from A and assuming that it touches the yield surface at B , we can write

$$\begin{aligned} s_x &= \bar{\varepsilon}_x^* + \cos \theta_A = 1 \\ s_{xy} &= -\tan \varphi \bar{\varepsilon}_x^* + \sin \theta_A = 0. \end{aligned}$$

We note also that $\theta_A = \pi - 2\varphi$ along the path AB . In the case $\gamma_m \rightarrow \infty$ the angle θ_A can be replaced by Φ and we obtain the condition for the maximal stress σ_x to be less or equal to σ_0

$$|\eta| \geq \frac{\sqrt{3(3+2m)}}{1+m} = \eta_{m(\infty)}.$$

Here again for a finite value of γ_m , the corresponding value $\eta_m = \eta_m(\gamma_m)$ is greater than $\eta_{m(\infty)}$, thus $\eta_m(\gamma_m) > \eta_{m(\infty)}$. After reaching the yield stress at B the stress path remains on the yield surface and at the instant of reversing the twist, the stress state is represented by point C which is a mirror image of point A with respect to the s_x -axis. When the elastic unloading occurs, the yield surface is reached again at the point D which is the mirror reflection of point B , Fig. 5a. The maximal value of the tensile stress s_{\max} reached in the course of deformation process is represented by points B and D . When $\eta = \eta_m$, then $s_{\max} = 1$ and points B and D merge on the s_x -axis.

Figure 6 presents the variation of angle difference $\varphi - \Phi$ for increasing values of η and different values of the Poisson ratio. It is seen that $\varphi - \Phi$ reaches a maximum for η close to 2 and then tends to 0. As far as this difference is always positive, for the initial elastic loading process, at the instance when the

yield surface is reached for the first time, one always observes an increase of the axial stress (compare Eq. (4.9) for $\theta = \varphi$ and Figs. 9–11). The characteristic material parameters and two limit values of η for different metallic materials are collected in Table 1¹⁾. It is seen that η_l and η_m vary within very small range.

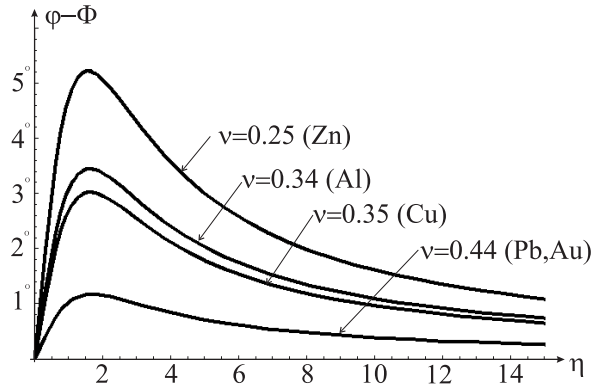


FIG. 6. Difference $\varphi - \Phi$ for varying η and different values of ν .

Table 1. Values of material parameters and two limit values of η for different metallic materials (values marked by a star specify the tensile strength). For Al-alloys, cast iron and steels, the yield stress strongly depends on the steel composition and the forming process.

Metal	E [GPa]	σ_0 [MPa]	ε_0 [%]	ν	m	η_m	η_l
Al	68.3	13–22	0.02–0.03	0.34	0.119	2.785	1.637
Al-alloy	70	40–320	0.06–0.45	0.33	0.128	2.771	1.631
Sn	54.3	34.5*	0.06*	0.36	0.103	2.812	1.649
Zn	86.9	110*	0.13*	0.25	0.200	2.661	1.581
Cu(annealed)	123	40–80	0.03–0.06	0.35	0.111	2.798	1.643
Pb	16.2	12.5*	0.08*	0.44	0.042	2.920	1.697
Ag	79.5	276*	0.35*	0.37	0.095	2.825	1.655
Ti	110	170	0.15	0.36	0.103	2.812	1.649
Au	80	138*	0.17*	0.44	0.042	2.920	1.697
cast iron	211	80–150	0.04–0.07	0.27	0.181	2.689	1.594
mild steel	210	130–350	0.06–0.17	0.29	0.163	2.716	1.606
stainless steel	210	500–680	0.24–0.33	0.3	0.154	2.730	1.612

Figure 5c presents the case when the yield point at B is reached by the elastic unloading path AB for $s_{xy}(B) > 0$ and similarly, the point D is reached for $s_{xy}(D) < 0$. This case corresponds to $\eta_l(\gamma_m) \leq \eta \leq \eta_m(\gamma_m)$. Figure 5d

¹⁾Material parameters in Table 1 are collected on the basis of *A concise encyclopedia of metallurgy*, A.D. MERRIMAN [Ed.] and *Vademecum of Material Science* [in Polish], W. DOMKE, WNT, Warszawa, 1982.

presents the stress path for which there is no elastic unloading and the whole deformation process is purely plastic. This occurs when $\eta \leq \eta_l(\gamma_m)$.

Let us now provide the solution for the half-cycle of the steady state of cyclic deformation presented in Fig. 5a. At the point A we have $\bar{\varepsilon}_x(A) = \bar{\varepsilon}_A$, $\bar{\gamma}_{xy}(A) = \bar{\gamma}_m$, $\bar{\varepsilon}_x = \bar{\varepsilon}_A + \Delta\bar{\varepsilon}_x$. Along the path portion AB the elastic deformation occurs and we have

$$(4.14) \quad s_x = \Delta\bar{\varepsilon}_x + \cos\theta_A,$$

$$(4.15) \quad s_{xy} = -\tan\varphi\Delta\bar{\varepsilon}_x + \sin\theta_A.$$

Along the stress path portion BC the elastic-plastic deformation occurs, and we have in view of (4.10)

$$\begin{aligned} \bar{E}_x/2 = \Delta\bar{\varepsilon}_x(\theta_C) &= \cos\theta_B - \cos\theta_A - f(-\theta_B) + f(-\theta_C) \\ &= \cos\theta_D - \cos\theta_A - f(\theta_D) + f(\theta_A) \end{aligned}$$

and finally

$$(4.16) \quad \bar{\gamma}_m = \frac{\eta}{2} (\cos\theta_D - \cos\theta_A - f(\theta_D) + f(\theta_A)).$$

On the other hand, when no elastic unloading occurs, this relation simplifies to

$$(4.17) \quad \bar{\gamma}_m = \frac{\eta}{2} (f(\theta_A) - f(-\theta_A)).$$

Equations (4.16) and (4.17) provide the solution for steady cyclic states. In fact, as $\theta_D = \theta_A - (\pi - 2\varphi)$, $\cos\theta_D = -\cos(\theta_A + 2\varphi)$, Eq. (4.16) can be rewritten in the form

$$(4.18) \quad \bar{\gamma}_m = \frac{\eta}{2} (-\cos(\theta_A + 2\varphi) - \cos\theta_A - f(\theta_A + 2\varphi - \pi) + f(\theta_A)).$$

This equation can be solved numerically for specified $\bar{\gamma}_m$ and η thus providing θ_A , θ_D and $\theta_B = -\theta_D$, $\theta_C = -\theta_A$. For a purely plastic regime Eq. (4.17) provides the solution for θ_A .

Now, let us specify the limit response curves $\eta_l = \eta_l(\gamma_m)$ and $\eta_m = \eta_m(\gamma_m)$ separating in the plane of process parameters η, γ_m the domains of different responses, with stress paths shown in Fig. 5. The curve $\eta_m = \eta_m(\gamma_m)$ separates the domains \mathcal{C} and \mathcal{B} . In the domain \mathcal{C} both the elastic unloading or reloading tensile paths AB and CD occur with reduction of maximal stress with respect to the limit value $\sigma_x = \sigma_0$, cf. Fig. 5a. In the domain \mathcal{B} , the elastic unloading and reloading paths AB and CD exist, but the maximal value of tensile stress equals σ_0 , cf. Fig. 5. The curve $\eta_l = \eta_l(\gamma_m)$ separates the domains \mathcal{B} and \mathcal{A} ,

where in the domain \mathcal{A} no elastic unloading or reloading occurs, cf. Fig. 5d. As for the case of purely plastic cycle there is $\theta_D = -\theta_A$, we have, in view of the relation $\theta_D = \theta_A - (\pi - 2\varphi)$, the value of $\theta_A = \pi/2 - \varphi = -\theta_D$ and the limit line $\eta_l = \eta_l(\gamma_m)$ is specified by the relation

$$\bar{\gamma}_m = \frac{\eta_l}{2} \left(f\left(\frac{\pi}{2} - \varphi\right) - f\left(\varphi - \frac{\pi}{2}\right) \right).$$

The response curve $\eta_m = \eta_m(\gamma_m)$ separating the domains \mathcal{C} and \mathcal{B} is specified by setting $\theta_D = 0$ and $\theta_A = \pi - 2\varphi$ into Eq. (4.16) what provides

$$\bar{\gamma}_m = \frac{\eta_m}{2} (1 + \cos(2\varphi) - f(0) + f(\pi - 2\varphi)).$$

Figure 7 provides the three response domains in the plane $(\eta, \gamma_m/\varepsilon_0)$. Let us note that the separating curves tend to asymptotic values $\eta_{l(\infty)}$ and $\eta_{m(\infty)}$ for $\gamma_m \rightarrow \infty$.

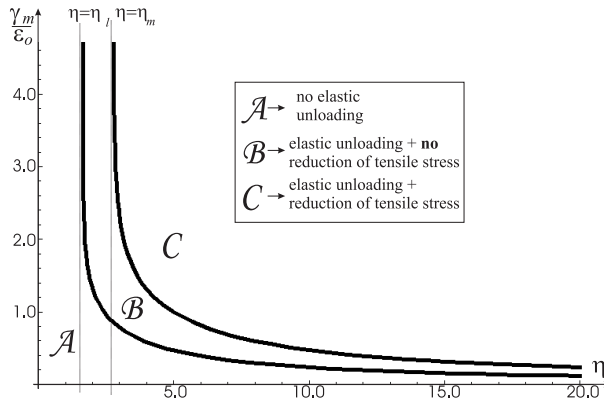


FIG. 7. The regimes \mathcal{A} , \mathcal{B} , \mathcal{C} of cyclic response in the plane of process parameters η , γ_m ($m = m_{Al} = 0.128$).

Let us note that for the regime \mathcal{C} where the elastic unloading or reloading occurs, we have

$$s_{\max} = \cos \theta_D = -\cos(\theta_A + 2\varphi), \quad s^* = \frac{\sin(\theta_A + \varphi)}{\sin \varphi}, \quad s_{\min} = \cos \theta_A$$

and for the remaining two regimes \mathcal{A} and \mathcal{B} there is

$$s_{\max} = s^* = 1, \quad s_{\min} = \cos \theta_A,$$

so the angle θ_A could be easily related to s_{\min} .

Figure 8 presents the distribution of isolines $s_{\max} = \text{const}$. The domains \mathcal{A} and \mathcal{B} for which $s_{\max} = 1$ is marked below the separating curve $\eta_m = \eta_{m(\infty)}$. It is seen that the isolines $s_{\max} = \text{const}$ tend to asymptotic values for $\gamma_m \rightarrow \infty$ and $\eta \rightarrow \infty$, satisfying the relations

$$\bar{\gamma}_m^{s_{\max}} = \frac{\sqrt{3(1-s_{\max}^2)}}{1+m}, \quad \eta_l^{s_{\max}} - \sqrt{3} \tan [\arccos(s_{\max}) - 2\varphi(\eta_m^{s_{\max}})] = 0.$$

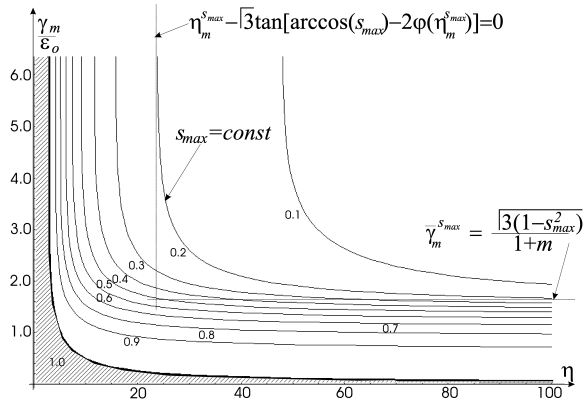


FIG. 8. Minimal values s_{\max} of the tensile stress in the plane of process parameters η , γ_m . Bold lines separate the regimes \mathcal{A} , \mathcal{B} , \mathcal{C} ($m = m_{Al} = 0.128$).

The typical axial and torsional cyclic responses for different values of η and $\bar{\gamma}_m$ are illustrated in Figs. 9–11.

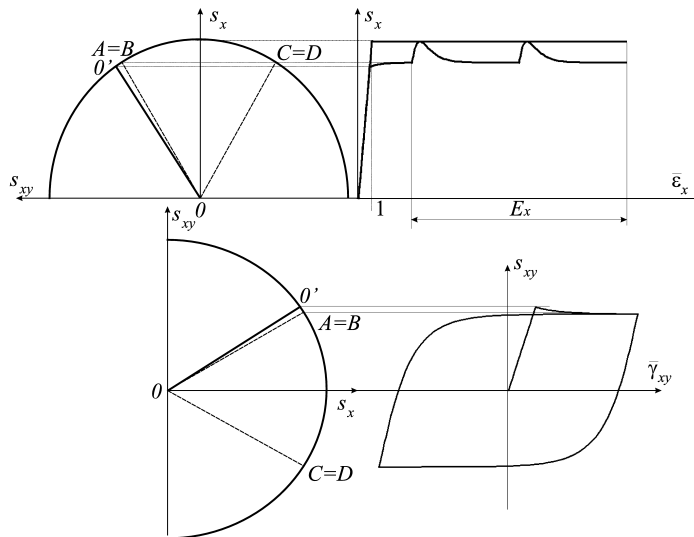


FIG. 9. Variation of the tensile stress path and the hysteresis loop of shear stress-strain response in the course of cyclic deformation, $\eta < \eta_l$ regime \mathcal{A} : no elastic unloading.

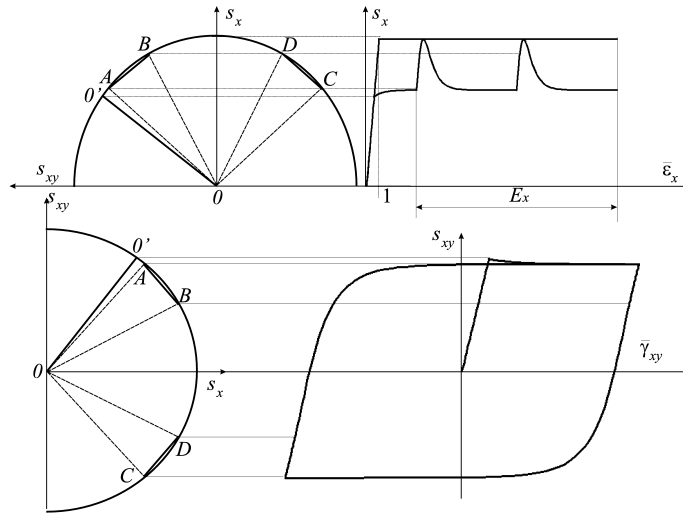


FIG. 10. Variation of the tensile stress path and the hysteresis loop of shear stress-strain response in the steady cyclic deformation, $\eta_l < \eta < \eta_m$ regime \mathcal{B} : elastic unloading and no reduction of s_{\max} .

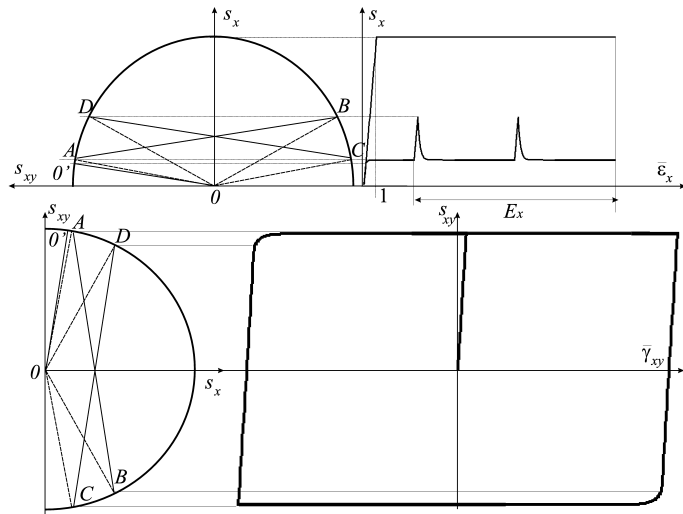


FIG. 11. Variation of the tensile stress path and the hysteresis loop of shear stress-strain response in the steady cyclic deformation, $\eta > \eta_m$ (regime \mathcal{C} : elastic unloading, maximal tensile stress reduction).

Consider now the plastic dissipation generated in one deformation cycle. Following (A.2), (A.3) and (A.4), we may calculate the total dissipation $\Delta\bar{D}$, and

the portions $\Delta\bar{D}_x$, $\Delta\bar{D}_{xy}$. Figure 12 presents the variation of dissipation increments for increasing values of η . It is seen that the total dissipation increment largely increases with respect to the dissipation increment in pure tension. However, the tensile dissipation increment decreases and tends to zero for increasing values of η .

The increment of plastic dissipation during one cycle when $\theta_A \rightarrow \Phi$ (for sufficiently large values of E_x and γ_m) may be calculated as a double increment of plastic dissipation during the half-cycle, so that

$$\Delta\bar{D}_{\text{cycle}} = 2(\bar{D}(\theta_A) - \bar{D}(\theta_D)) = 2(\bar{D}(\theta_A) - \bar{D}(\theta_A - \pi + 2\varphi))$$

for an elastic-plastic half-cycle and

$$\Delta\bar{D}_{\text{cycle}} = 2(\bar{D}(\theta_A) - \bar{D}(-\theta_A))$$

for a totally plastic semicycle. Let us note that the angle θ_A is uniquely related to γ_m , η and E_x for the steady cycle, Eqs. (4.17), (4.18).

Similarly we may calculate the increment of the axial plastic strain $\bar{\varepsilon}_x^P$ during one steady cycle respectively for two regimes, so we have

$$\Delta\bar{\varepsilon}_{\text{cycle}}^P = 2(\bar{\varepsilon}_x^P(\theta_A) - \bar{\varepsilon}_x^P(\theta_A - \pi + 2\varphi)),$$

$$\Delta\bar{\varepsilon}_{\text{cycle}}^P = 2(\bar{\varepsilon}_x^P(\theta_A) - \bar{\varepsilon}_x^P(-\theta_A)).$$

Let the ratio $\delta = \frac{\Delta\bar{D}_{\text{cycle}}}{\Delta\bar{\varepsilon}_{\text{cycle}}^P}$ of a plastic work increment and a plastic strain increment during one cycle be treated as a energy-based measure of expense of the plastic extension process. For the pure tension this *expense coefficient* δ equals one.

It would be interesting to find the upper limit value of δ for arbitrary values of η but for $\gamma_m \rightarrow \infty$ what is equivalent to $\theta_A \rightarrow \Phi$. We obtain (as compared to the results (3.9)–(3.11))

$$\begin{aligned} (4.19) \quad \delta_l &= \lim_{\theta_A \rightarrow \Phi} \frac{\Delta\bar{D}_{\text{cycle}}}{\Delta\bar{\varepsilon}_{\text{cycle}}^P} = \lim_{\theta_A \rightarrow \Phi} \frac{\bar{D}(\theta_A) - \bar{D}(\theta_A - \pi + 2\varphi)}{\bar{\varepsilon}_x^P(\theta_A) - \bar{\varepsilon}_x^P(\theta_A - \pi + 2\varphi)} \\ &= \lim_{\theta_A \rightarrow \Phi} \frac{\frac{d\bar{D}}{d\theta}}{\frac{d\bar{\varepsilon}^P}{d\theta}} = \frac{1}{\cos\Phi} = \sqrt{1 + \frac{\eta^2}{3}} \end{aligned}$$

and similarly

$$(4.20) \quad \lim_{\theta_A \rightarrow \Phi} \frac{\Delta\bar{D}_{x\text{cycle}}}{\Delta\bar{\varepsilon}_{\text{cycle}}^P} = \cos\Phi = \frac{1}{\sqrt{1 + \frac{\eta^2}{3}}},$$

$$(4.21) \quad \lim_{\theta_A \rightarrow \Phi} \frac{\Delta \bar{D}_{xy}^{\text{cycle}}}{\Delta \bar{\epsilon}_{\text{cycle}}^P} = \frac{1}{\cos \Phi} - \cos \Phi = \frac{\frac{1}{3}\eta^2}{\sqrt{1 + \frac{\eta^2}{3}}}$$

Figure 12a presents the variation of the expense coefficient for varying values of η and E_x . Figures 12b,c present the evolution of axial and torsional expense coefficients. The bold lines present the limit values derived analytically, cf. Eqs. (4.19)–(4.21). It is seen that the total dissipation always increases for the combined process, however the axial dissipation decreases remarkably for increasing values of η and γ_m .

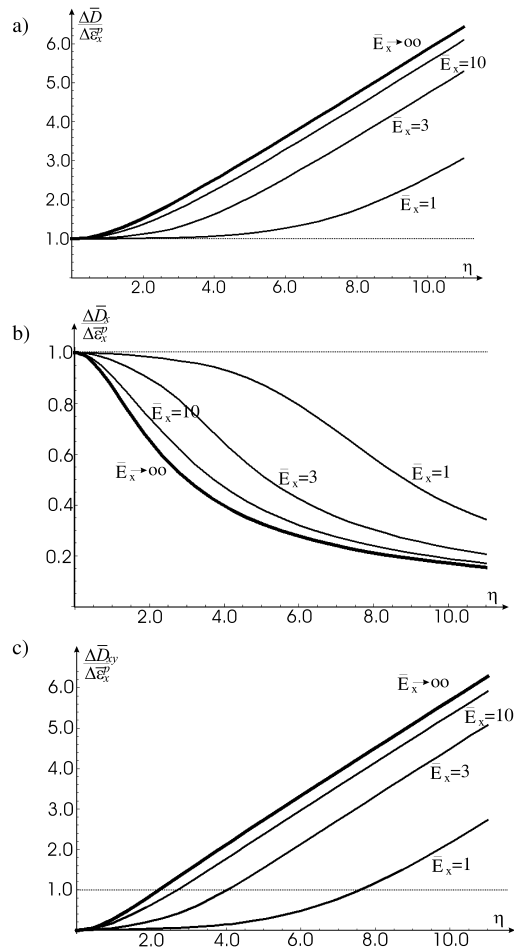


FIG. 12. a) Variation of the ratio of total plastic dissipation increment per cycle and the axial plastic strain increment (expense coefficient δ) with E_x and η , b) variation of axial expense coefficient c) variation of torsional expense coefficient.

4.3. Harmonic shear strain control: incremental relations

Consider now the harmonic shear strain control specified by (2.2), accompanied by the progressive axial extension, thus

$$(4.22) \quad \dot{\varepsilon}_x = \dot{\alpha}, \quad \frac{\dot{\gamma}_{xy}}{\dot{\varepsilon}_x} = \eta \frac{\pi}{2} \cos \left(2\pi \frac{\varepsilon_x}{E_x} \right).$$

For the elastic regime, the incremental (or rate) equations are

$$(4.23) \quad \dot{\sigma}_x = E \dot{\varepsilon}_x, \quad \dot{\tau}_{xy} = G \eta \frac{\pi}{2} \cos \left(2\pi \frac{\varepsilon_x}{E_x} \right) \dot{\varepsilon}_x,$$

and for the elastic-plastic regime we have

$$(4.24) \quad \dot{\sigma}_x = E \left(\dot{\varepsilon}_x - \dot{\lambda} \frac{\sigma_x}{\sigma_0} \right), \quad \dot{\tau}_{xy} = G \left(\eta \frac{\pi}{2} \cos \left(2\pi \frac{\varepsilon_x}{E_x} \right) \dot{\varepsilon}_x - \dot{\lambda} \frac{3\tau_{xy}}{\sigma_0} \right).$$

The yield condition (3.1) and the consistency condition $\dot{F} = 0$ provide

$$(4.25) \quad \dot{\lambda} = \sigma_0 \frac{E\sigma_x + 3G\eta \frac{\pi}{2} \cos \left(2\pi \frac{\varepsilon_x}{E_x} \right) \tau_{xy}}{E\sigma_x^2 + 9G\tau_{xy}^2} \dot{\varepsilon}_x$$

and the relations (4.24) can be written in the form

$$(4.26) \quad \begin{aligned} \dot{\sigma}_x &= E \left(1 - \frac{E\sigma_x + 3G\eta \frac{\pi}{2} \cos \left(2\pi \frac{\varepsilon_x}{E_x} \right) \tau_{xy}}{E\sigma_x^2 + 9G\tau_{xy}^2} \sigma_x \right) \dot{\varepsilon}_x, \\ \dot{\tau}_{xy} &= G \left(\eta \frac{\pi}{2} \cos \left(2\pi \frac{\varepsilon_x}{E_x} \right) - \frac{E\sigma_x + 3G\eta \frac{\pi}{2} \cos \left(2\pi \frac{\varepsilon_x}{E_x} \right) \tau_{xy}}{E\sigma_x^2 + 9G\tau_{xy}^2} 3\tau_{xy} \right) \dot{\varepsilon}_x. \end{aligned}$$

Introducing the trigonometric stress representation (4.5) and the notation (4.8), the incremental relations (4.26) can be presented as follows:

$$(4.27) \quad \frac{\sigma_0}{3G} \dot{\theta} = \frac{\frac{\sqrt{3}\eta}{3} \frac{\pi}{2} \cos \left(2\pi \frac{\varepsilon_x}{E_x} \right) \cos \theta - \sin \theta}{1 + \left(\frac{3G}{E} - 1 \right) \sin^2 \theta} \dot{\varepsilon}_x$$

or

$$(4.28) \quad d\bar{\varepsilon}_x = \frac{1}{1+m} \frac{1+m(\sin\theta)^2}{\tan\Phi \frac{\pi}{2} \cos\left(\frac{\bar{\varepsilon}_x}{\bar{E}_x}\right) \cos\theta - \sin\theta} d\theta,$$

where $\bar{\varepsilon}_x = \varepsilon_x/\varepsilon_0$. Equation (4.28) can be integrated numerically. The elastic unloading condition is now $\dot{\lambda} = 0$ and

$$(4.29) \quad \dot{F} = \sigma_0 \left[\cos\theta + (1+m) \frac{\pi}{2} \frac{\eta}{\sqrt{3}} \cos\left(2\pi \frac{\varepsilon_x}{E_x}\right) \right] \dot{\varepsilon}_x \leq 0.$$

Introducing the notation

$$\begin{aligned} \tan\left[\Phi\left(\frac{\bar{\varepsilon}_x}{\bar{E}_x}\right)\right] &= \frac{\pi}{2} \frac{\sqrt{3}\eta}{3} \cos\left(2\pi \frac{\bar{\varepsilon}_x}{\bar{E}_x}\right), \\ \tan\left[\varphi\left(\frac{\bar{\varepsilon}_x}{\bar{E}_x}\right)\right] &= (1+m) \frac{\pi}{2} \frac{\eta}{\sqrt{3}} \cos\left(2\pi \frac{\bar{\varepsilon}_x}{\bar{E}_x}\right) = \frac{\dot{s}_{xy}^e}{\dot{s}_x^e} \end{aligned}$$

it is obtained from (4.29) for the neutral, limit process

$$\cos(\theta - \varphi) = 0, \quad \theta - \varphi = \pm \frac{\pi}{2},$$

so the stress trajectory in the s_x, s_{xy} -plane at the instant of unloading is tangential to the yield surface. The elastic stress rates \dot{s}_{xy}^e and \dot{s}_x^e then specify the angle φ .

The reverse point of the axial stress oscillation is specified by the condition $ds_x/d\varepsilon_x = 0$ and then

$$\sin\theta \sin(\Phi - \theta) = 0, \quad \text{so that} \quad \theta = \Phi$$

and the tensile stress reduction occurs when $\Phi < \theta$.

The typical stress paths are presented in Figs. 13–15. Similarly as for the piecewise linear shear strain control, the response regimes \mathcal{A} , \mathcal{B} , \mathcal{C} will occur depending on γ_m and η .

Figure 13 presents the cyclic material response for $\eta = 6$, $\gamma_{m3}/\varepsilon_0 = 4.62$ when the cyclic process is composed of elastic and elastic-plastic portions with the reduction of maximal axial stress (regime \mathcal{C}). Figure 14 presents the cyclic response for $\eta = 6$, $\gamma_{m2}/\varepsilon_0 = 9.24$ when the elastic and elastic-plastic portions occur with no reduction of maximal axial stress (regime \mathcal{B}). Figure 15 for $\eta = 6$, $\gamma_{m1}/\varepsilon_0 = 0.924$ presents the response for small amplitude value and no maximal stress reduction.

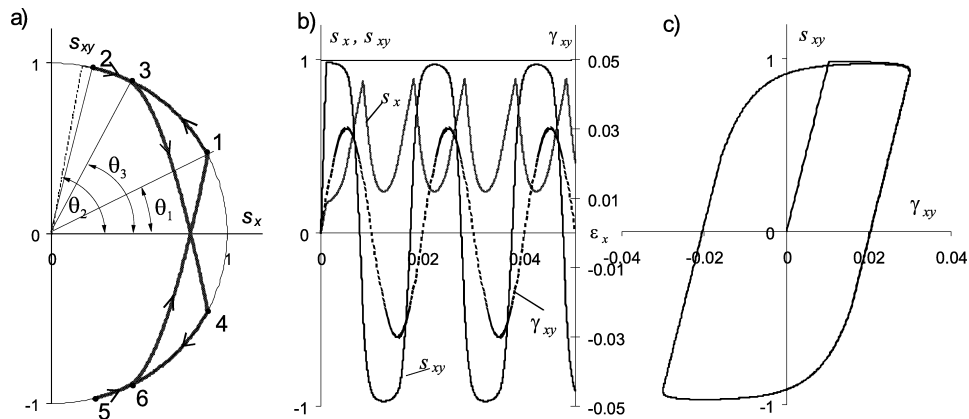


FIG. 13. Harmonic shear strain control with maximal axial stress reduction and elasto-plastic response ($\eta = 6$, $\gamma_m/\varepsilon_0 = 4.62$) a) cyclic stress path, b) variation of axial and shear stress and shear strain, c) torsional hysteresis loop.

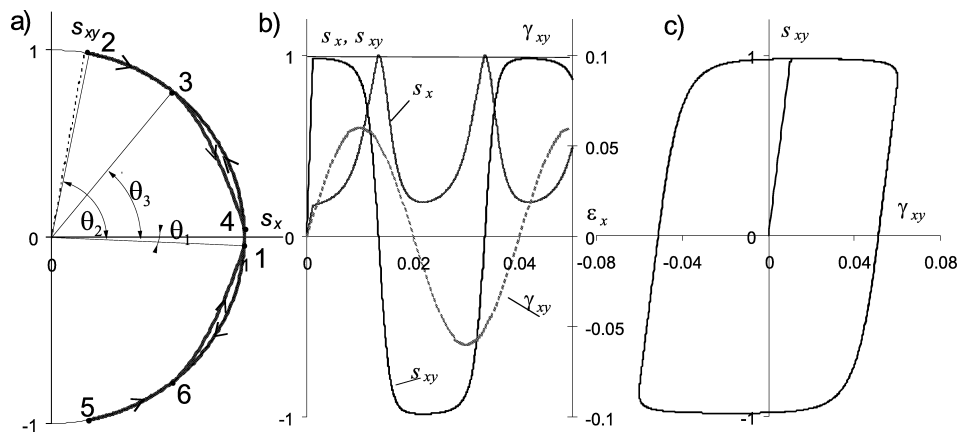


FIG. 14. Harmonic shear strain control with no maximal axial stress reduction and elasto-plastic response ($\eta = 6$, $\gamma_m/\varepsilon_0 = 9.24$) a) cyclic stress path, b) variation of axial and shear stress and shear strain c) torsional hysteresis loop.

Figure 16 presents the cyclic response diagram in the plane $\gamma_m/\varepsilon_0, \eta$. It is seen that the line separating the regimes $\mathcal{A} + \mathcal{B}$ and \mathcal{C} differs essentially from that generated for a piecewise linear control. In fact, for instance with $\eta = 6$ and increasing γ_m/ε_0 , we intersect the domain \mathcal{C} at two points for small and large values of γ_m/ε_0 . Thus, there is no reduction of maximal value of s_x for sufficiently small values of $\gamma_m \leq \gamma_{m1}$ and for sufficiently large values $\gamma_m \geq \gamma_{m2}$. For a piecewise linear control the separating lines tend to asymptotic values of γ_m/ε_0 and η , cf. Fig. 7. The diagrams shown in Figs. 13, 14 and 15 are presented

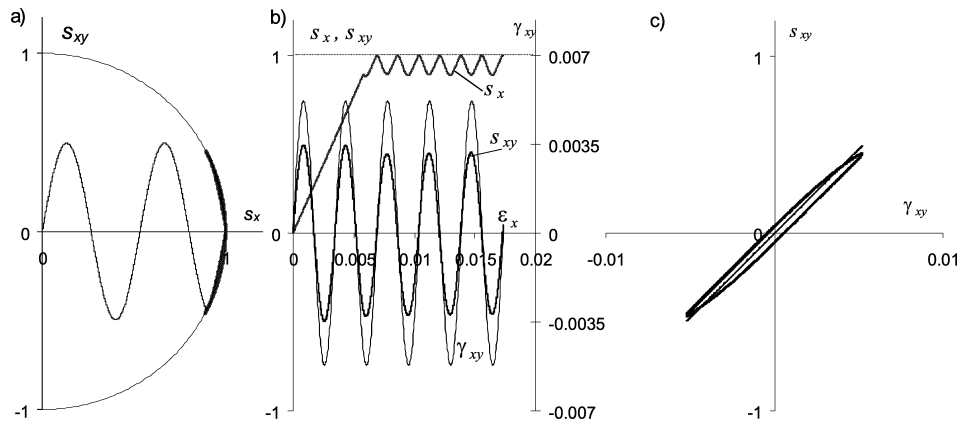


FIG. 15. Harmonic shear strain control with no maximal axial stress reduction and plastic response ($\eta = 6$, $\gamma_m/\varepsilon_0 = 0.924$) a) cyclic stress path, b) variation of axial and shear stress and shear strain, c) torsional hysteresis loop.

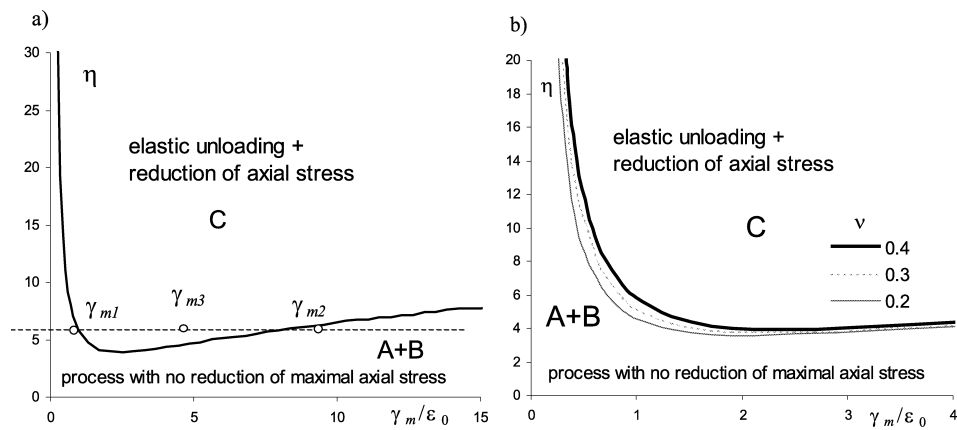


FIG. 16. The response diagram in the plane $\gamma_m/\varepsilon_0, \eta$ specifying domains $\mathcal{A} + \mathcal{B}$ and \mathcal{C} of no-reduction and reduction of maximal axial stress a) diagram for large values of γ_m/ε_0 , b) diagram for small values of γ_m/ε_0 .

for the values $\gamma_m = \gamma_{m1}$, γ_{m2} and γ_{m3} marked in Fig. 16. It is also demonstrated that the periodic shear strain variation exhibits phase shift with respect to the shear stress variation.

Figure 17 presents the comparative diagrams of axial stress variation for piecewise linear and harmonic shear strain control for the same values of γ_m and η . It is seen that much greater axial stress reduction occurs for piecewise-linear control for larger values of γ_m .

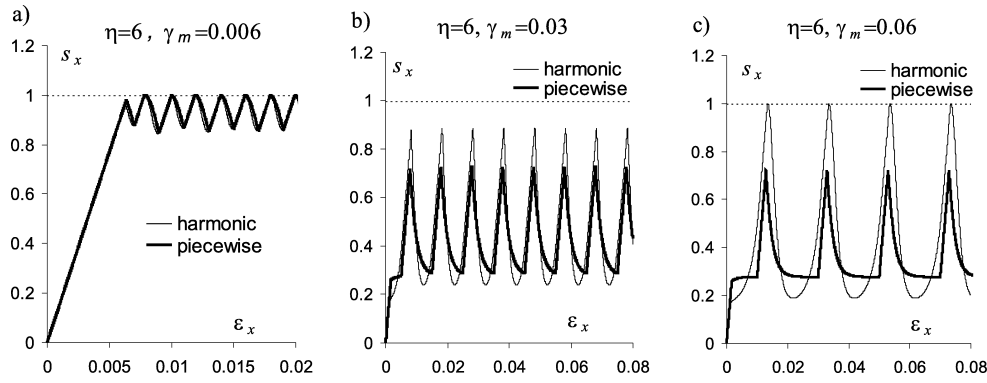


FIG. 17. Comparison of the tensile stress paths for piecewise linear and harmonic shear strain controls ($E = 77000$ MPa, $\nu = 0.4$, $\sigma_0 = 500$ MPa, $\eta = 6$), a) $\gamma_{m1} = 0.006$, b) $\gamma_{m3} = 0.03$, c) $\gamma_{m2} = 0.06$. Relative parameter values: $\varepsilon_0 = \sigma_0/E \sim 0.0065$, $\gamma_m/\varepsilon_0 = 0.924; 4.62; 9.24$.

5. Approximate cyclic solution for a cylinder

In this section we shall discuss the approximate solution for the steady cyclic state in a cylinder subjected to axial tension or compression, combined with cyclic torsion of a specified angular amplitude. We assume that the cylinder is composed of thin-walled tubes of varying radii and neglect the radial tube interaction, Fig. 18. Assuming the plane cross-section and material incompressibility, the strain tensor is expressed in the cylindrical coordinate system

$$\varepsilon_x = \varepsilon, \quad \gamma_{x\theta} = \vartheta_r, \quad \varepsilon_r = \varepsilon_\theta = -\frac{1}{2}\varepsilon$$

and the non-vanishing strain rate components are

$$\dot{\varepsilon}_x = \dot{\varepsilon}, \quad \dot{\gamma}_{x\theta} = \dot{\vartheta}_r, \quad \dot{\varepsilon}_r = \dot{\varepsilon}_\theta = -\frac{1}{2}\dot{\varepsilon}.$$

Assume the linear variation of shear strain with the radius r and constant tensile strain of each tube, so that

$$\gamma_{x\theta}(r) = \gamma_{x\theta}^R \frac{r}{R}, \quad \varepsilon_x(r) = \varepsilon_x, \quad r = r_0 \exp(\varepsilon_r), \quad \dot{r} = r\dot{\varepsilon}_r,$$

where R is the actual outer radius of the cylinder. The strain rates are

$$\dot{\varepsilon}_x = \dot{\alpha} = \text{const}, \quad \dot{\varepsilon}_r = -\frac{1}{2}\dot{\varepsilon} = \text{const}, \quad \dot{\gamma}_{x\theta}(r) = \dot{\gamma}_{x\theta}^R \frac{r}{R}.$$

Similarly to the case of a thin-walled tube, two different shear strain programs are considered: piecewise linear and harmonic, so we have

$$\dot{\gamma}_{x\theta}^R = \eta^R \dot{\varepsilon}_x, \quad \text{or} \quad \dot{\gamma}_{x\theta}^R = \eta^R \frac{\pi}{2} \cos\left(2\pi \frac{\varepsilon_x}{E_x}\right) \dot{\varepsilon}_x.$$

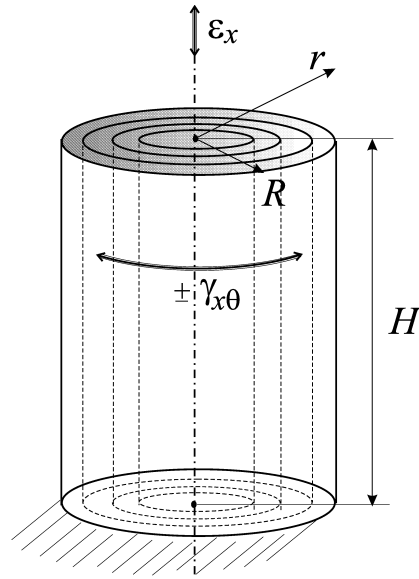


FIG. 18. Cylinder geometry.

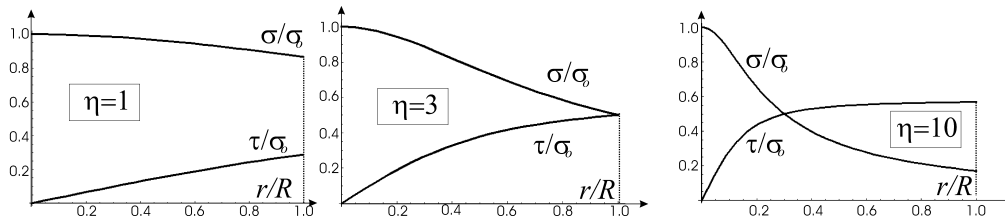
5.1. Piecewise linear shear strain control: rigid-plastic model

Assuming the rigid-perfectly plastic model, and using the solution (3.5) for a tube, we can present the stress distribution in the cylinder

$$(5.1) \quad \sigma_x(\bar{r}) = \frac{\sigma_0}{\sqrt{1 + \frac{\eta^2 \bar{r}^2}{3}}}, \quad \tau_{x\theta}(\bar{r}) = \pm \frac{\eta}{3} \frac{\sigma_0 \bar{r}}{\sqrt{1 + \frac{\eta^2 \bar{r}^2}{3}}},$$

$$\text{where } \bar{r} = \frac{r}{R}.$$

The stress distribution for $\eta = 1, 3$ and 10 is shown in Fig. 19.

FIG. 19. Variation of axial stress and shear stresses in a cylinder for $\eta = 1, 3, 10$.

Integrating the axial and shear stresses (5.1) over the actual cross-section of the cylinder, we obtain

$$F = F_0 \frac{6}{\eta^2} \left(\sqrt{1 + \frac{\eta^2}{3}} - 3 \right), \quad M = M_0 \frac{\sqrt{3}}{\eta^3} \left((\eta^2 - 6) \sqrt{1 + \frac{\eta^2}{3}} + 6 \right),$$

where $F_0 = F(\eta = 0)$ is the axial force in pure tension and $M_0 = M(\eta \rightarrow \infty)$ is the twisting moment in pure torsion, so that

$$F_0 = \pi R^2 \sigma_0, \quad M_0 = \frac{\sqrt{2}}{3\sqrt{3}} \pi R^3 \sigma_0.$$

Figure 20 presents the evolution of F/F_0 and M/M_0 in the course of cyclic deformation. It is seen that the axial force and the torsional hysteretic loop depend only on the value of parameter η . Figure 21 presents the variation of F/F_0 and $|M|/M_0$ with η . It is seen that the axial force decreases and the torsional moment amplitude increases with η .

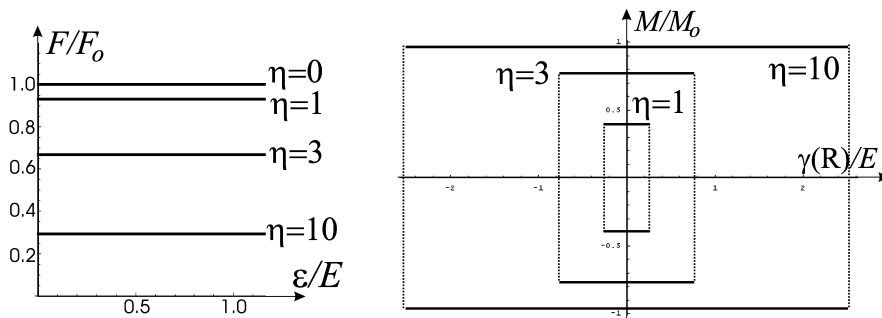


FIG. 20. The cross-sectional force and moment variation in the steady cyclic state.

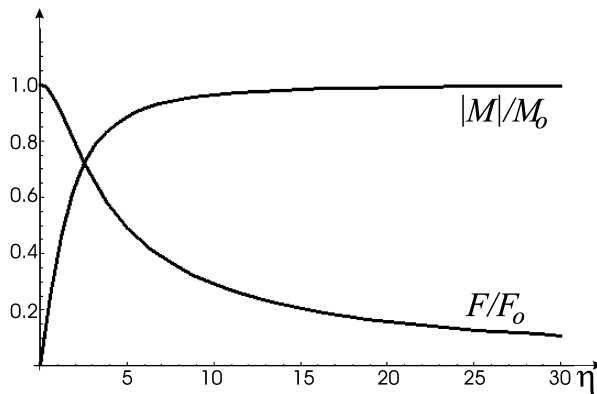


FIG. 21. Variation of axial force and twisting moment with the parameter η .

5.2. Harmonic control of shear strain: rigid-plastic model

For the harmonic variation of γ_{xy} , the stress components follow from the solution for a tube, Eq. (3.7), so we have

$$(5.2) \quad \begin{aligned} \sigma_x(\bar{r}) &= \frac{\sqrt{3}\sigma_0}{\sqrt{3 + \eta^2\bar{r}^2\frac{\pi^2}{4}\cos^2(2\pi e)}}, \\ \tau_{x\theta}(\bar{r}) &= \pm \frac{\sqrt{3}\sigma_0\bar{r}\eta\frac{\pi}{2}\cos(2\pi e)}{3\sqrt{3 + \eta^2\bar{r}^2\frac{\pi^2}{4}\cos^2(2\pi e)}}, \end{aligned}$$

where $e = \varepsilon_x/E_x$. Figure 22 presents the stress variation within the cylinder for increasing values of e , and the assumed value $\eta = 3$.

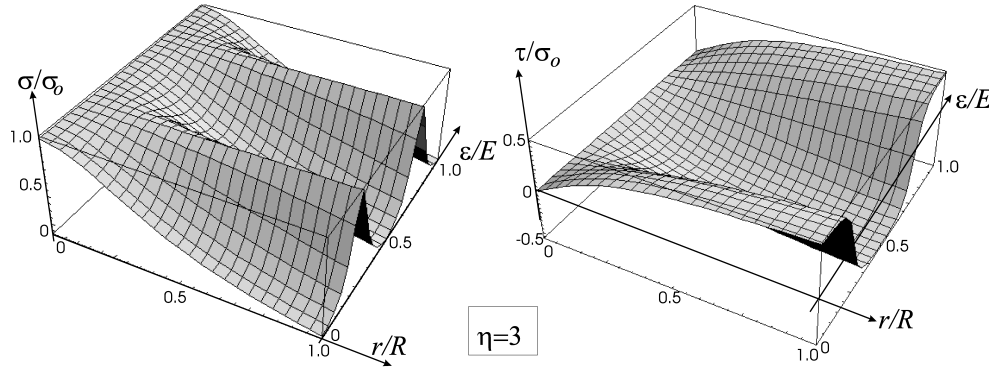


FIG. 22. The axial and shear stress distribution in cylinder for $\eta = 3$.

The cross-sectional axial force and twisting moment are expressed as follows:

$$\begin{aligned} F &= F_0 \frac{6}{\eta^2 \frac{\pi^2}{4} \cos^2(2\pi e)} \left(\sqrt{1 + \frac{1}{3} \eta^2 \frac{\pi^2}{4} \cos^2(2\pi e)} - 3 \right), \\ M &= M_0 \frac{\sqrt{3}}{\eta^3 \frac{\pi^3}{16} \cos^3(2\pi e)} \left((\eta^2 \frac{\pi^2}{4} \cos^2(2\pi e) - 6) \sqrt{1 + \frac{1}{3} \eta^2 \frac{\pi^2}{4} \cos^2(2\pi e)} + 6 \right). \end{aligned}$$

Variation of F/F_0 and M/M_0 in the course of steady cyclic deformation is presented in Fig. 23. It is seen that the axial force reaches its maximum equal to F_0 and its minimum value strongly depends on η .

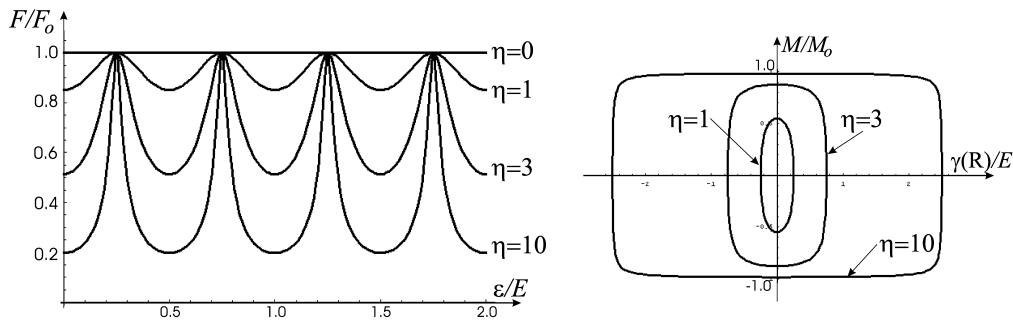


FIG. 23. Variation of axial force and twisting moment in the steady cyclic state for different values of η .

5.3. Piecewise linear shear strain control: elastic-plastic model

To simplify the analysis, we shall treat the cylinder as a discrete set of thin-walled tubes and neglect their radial interaction. The resulting axial force and torsional moment are obtained by summing up and averaging the stress contributions of consecutive tubes. Referring to Fig. 24, it is seen that depending on the value of radius r and sufficiently large values of η , the tubes can correspond to the regimes \mathcal{A} , \mathcal{B} , and \mathcal{C} . Thus in the external cylinder portion $r_2 \leq r \leq R$, the regime \mathcal{C} occurs with elastic unloading and maximal axial stress reduction, but in the central cylinder portion $0 \leq r \leq r_1$ the regime \mathcal{A} occurs with no elastic unloading during the steady cyclic deformation. In the intermediate portion $r_1 \leq r \leq r_2$ the regime \mathcal{B} occurs with no reduction of maximal tensile stress.

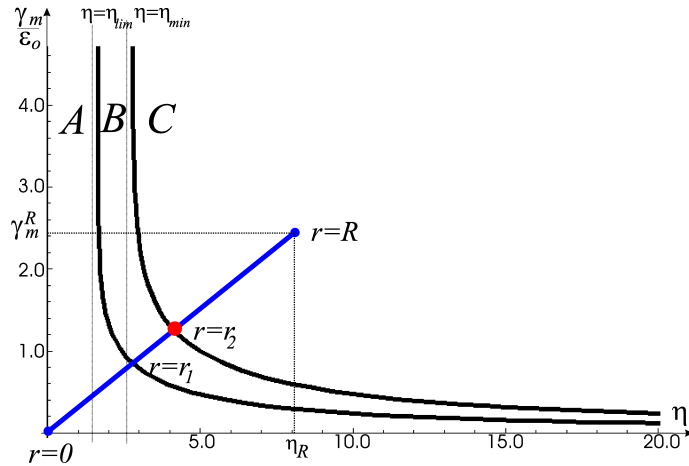


FIG. 24. Three different stress regimes within a cylinder subjected to monotonic extension and cyclic torsion.

6. Concluding remarks

The present paper provides the analysis of cyclic deformation modes for a tube or cylinder subjected to axial extension or compression with a specified rate, assisted by cyclic torsion of specified strain rate and amplitude. The fundamental process parameters are the ratio of rates of shear and axial strains η and the shear strain amplitude γ_m . Three different stress regimes have been detected and analyzed in detail. The response domains in the plane of process parameters are specified and plotted in the form of diagrams resembling the familiar Bree diagrams specifying the shakedown, alternating plasticity and ratchetting domains for structural elements under load control and a perfectly plastic material response. It is demonstrated that considerable axial force reduction can be attained for sufficiently large values of η and γ_m . However, the plastic energy dissipation in the process is always larger with respect to the pure axial extension or compression for a specified total elongation or shortening of the cylinder. The response for piecewise linear and harmonic shear strain control is illustrated by presenting the cyclic stress path and stress-strain diagrams. The application of material hardening models combined with dynamic recovery effects would provide different results and prediction of reduced energy dissipation. This topic will be the subject of a separate study and confrontation with experimental data. The problem of microstructure evolution in the course of cyclic loading, especially fine-grained structure generation will also be analysed. The present paper provides the fundamental clarification of cyclic deformation modes and their dependence on process parameters.

Appendix A.

Using trigonometric stress representation (4.5), the axial component of plastic strain $\dot{\varepsilon}_x^p = \dot{\lambda} \cos \theta$. Integrating we obtain for $\eta = \pm|\eta|$

$$\bar{\varepsilon}_x^p = C_\varepsilon - \frac{\cos \Phi}{(1+m) \cos \varphi} \left[\cos(\varphi - \Phi \pm \theta) + \cos(\varphi - \Phi) \cos \Phi \ln \left| \tan \left(\frac{\Phi \pm \theta}{2} \right) \right| \right]$$

where C_ε denotes the integration constant.

Now, let us specify the rate of plastic dissipation. During one cycle of deformation the elastic work vanishes and the work of external loading is dissipated. We have

$$(A.1) \quad \dot{D} = \sigma_x \dot{\varepsilon}_x^p + \tau_{xy} \dot{\gamma}_{xy}^p = \sigma_0 \dot{\lambda} = \dot{D}_x + \dot{D}_{xy}.$$

In view of (4.5) and (4.3) we obtain

$$\dot{D} = \frac{\sigma_0^2}{E(1+m)} \frac{\cos \Phi}{\cos \varphi} \frac{\cos(\varphi \mp \theta)}{\sin(\pm \Phi - \theta)} \dot{\theta}$$

and $\dot{D}_x = \sigma_0 \dot{\lambda} \cos^2 \theta$, $\dot{D}_{xy}^p = \sigma_0 \dot{\lambda} \sin^2 \theta$. Denoting $\bar{D} = D/D_0$, ($D_0 = \sigma_0 \varepsilon_0$) and integrating (A.1), we obtain for $\eta = \pm|\eta|$

$$(A.2) \quad \bar{D}(\theta) = C_w - \frac{\cos \Phi}{(1+m) \cos \varphi} [\cos(\varphi - \Phi) \ln |\sin(\Phi \pm \theta)| \pm \theta \sin(\varphi - \Phi)]$$

where C_w denotes the integration constants calculated from the accumulated value in the previous cycles. The tensile and torsional dissipated energies are

$$(A.3) \quad \bar{D}_x(\theta) = C_{wx} - \frac{1}{4} \frac{\cos \Phi}{(1+m) \cos \varphi} \left[\cos(\pm\varphi \mp \Phi - 2\theta) + A(\pm\Phi, \pm\varphi) \ln |\sin(\pm\Phi - \theta)| + \theta B(\pm\Phi, \pm\varphi) \right],$$

where

$$A(\Phi, \varphi) = \cos(\varphi + \Phi) + \cos(\varphi - 3\Phi) + 2 \cos(\varphi - \Phi),$$

$$B(\Phi, \varphi) = \sin(\varphi - 3\Phi) + 2 \sin(\varphi - \Phi) - \sin(\varphi + \Phi)$$

and

$$(A.4) \quad \bar{D}_{xy}(\theta) = C_{wxy} + \frac{1}{4} \frac{\cos \Phi}{(1+m) \cos \varphi} \left[\cos(\pm\varphi \mp \Phi - 2\theta) + C(\pm\Phi, \pm\varphi) \ln |\sin(\pm\Phi - \theta)| + \theta D(\pm\Phi, \pm\varphi) \right],$$

where

$$C(\Phi, \varphi) = \cos(\varphi + \Phi) + \cos(\varphi - 3\Phi) - 2 \cos(\varphi - \Phi),$$

$$D(\Phi, \varphi) = \sin(\varphi - 3\Phi) - 2 \sin(\varphi - \Phi) - \sin(\varphi + \Phi).$$

Acknowledgment

The research presented in this paper was supported by the National Research Council (KBN) grant No PBZ-KBN-102/TO8/2003.

References

1. Z.S. BASIŃSKI and P.J. JACKSON, *The instability of the work hardening state (I) – slip in extraneously deformed crystals*, Phys. Stat. Sol., **9**, 805, 1965.
2. W. BOCHNIAK and A. KORBEL, *Extrusion of CuZn39Pb2 alloy by the KOBO method*, Eng. Trans., **47**, 351–367, 1999.

3. W. BOCHNIAK and A. KORBEL, *Plastic flow of aluminium extruded, under complex conditions*, Mat. Sci. Technol., **16**, 664–674, 2000.
4. W. BOCHNIAK and A. KORBEL, *KOBO-type forming: forging of metals under complex conditions of the process*, J. Mat. Process. Technol., **134**, 120–134, 2003.
5. J.L. CHABOCHE, *On some modifications of kinematic hardening to improve the description of ratchetting effects*, Int. J. Plast., **7**, 661–678, 1991.
6. F. GROSSMAN and J. PAWLICKI, *The yield stress in the conditions of combined loadings* [in Polish], Proc. XII Conf. KomPlastTech. (Informatics in Metal Technology), Silesian Techn. Univ., pages 253–258, 2005.
7. P.J. JACKSON and Z.S. BASIŃSKI, *The effect of extraneous deformation on strain hardening in Cu single crystals*, Appl. Phys. Lett., **6**, 148, 1965.
8. L.F. COFFIN JR, *Low-cycle-fatigue: a review*, Appl. Mat. Res., **1**, 129–141, 1962.
9. G.Z. KANG, Q. GAO, and X.J. YANG, *A visco-plastic constitutive model incorporated with cyclic hardening for uniaxial/multiaxial ratchetting of SS 304 stainless steel at room temperature*, Mech. Mater., **34**, 521–531, 2002.
10. A.R. KHOEI and N. JAMALI, *On the implementation of a multisurface kinematic hardening plasticity and its applications*, Int. J. Plast., **21**, 1741–1770, 2005.
11. L.X. KONG and P.D. HODGSON, *Constitutive modeling of extrusion of lead with cyclic torsion*, Mat. Sci. Eng. A, **276**, 32–38, 2000.
12. L.X. KONG, P.D. HODGSON, and B. WANG, *Development of constitutive models for metal forming with cyclic strain softening*, J. Mat. Process. Technol., **89–90**, 44, 1999.
13. A. KORBEL and W. BOCHNIAK, *Refinement and control of the metal structure elements by plastic deformation*, Scripta Materialia, **51**, 755–759, 2004.
14. Z. MRÓZ, *On the description of anisotropic workhardening*, J. Mech. Phys. Solids, **15**, 163–175, 1967.
15. Z. MRÓZ and P. RODZIK, *On multisurface and integral description of anisotropic hardening evolution of metals*, Eur. J. Mech. A/Solids, **15**, 1–28, 1996.
16. N. OHNO and J.D. WANG, *Kinematic hardening rules for simulation of ratchetting behaviour*, Europ. J. Mech./A Solids, **13**, 519–531, 1994.
17. L. PORTIER, S. CALLOCH, D. MARQUIS, and P. GEYER, *Ratchetting under tension-torsion loadings: experiments and modeling*, Int. J. Plast., **16**, 303–335, 2000.
18. W. TRĄMPCZYŃSKI and Z. MRÓZ, *Anisotropic hardening model and its application to cyclic loading*, Int. J. Plast., **8**, 925–946, 1992.

Received October 3, 2005; revised version March 28, 2006.
